Two-dimensional elastic wave propagation analysis in finite length FG thick hollow cylinders with 2D nonlinear grading patterns using MLPG method

S.M. Moussavinezhad[1]**, Farzad Shahabian**[1]**, Seyed Mahmoud Hosseini**[2,3]

Abstract: In this article, the propagation of elastic wave is studied in two dimensional functionally graded thick hollow cylinder with finite length subjected to mechanical shock loading, considering two dimensional variations for mechanical properties. The meshless local Petrov-Galerkin (MLPG) method is developed to solve the boundary value problem. The Newmark finite difference method is used to treat the time dependence of the variables for transient problems. The FG cylinder is considered to be under axisymmetric conditions. The mechanical properties of FG cylinder are assumed to vary across thickness and length of FG cylinder in terms of two dimensional volume fractions as nonlinear functions. A weak formulation for the set of governing equations is transformed into local integral equations on local sub-domains by using a Heaviside test function. Nodal points are regularly distributed along the radius and length of the cylinder and each node is surrounded by a circular sub-domain to which a local integral equation is applied. The wave fronts of displacements are illustrated for various values of volume fraction exponents in 2D domain at various time intervals. The 2D propagation of elastic wave can be tracked through radial and axial directions in 2D functionally graded cylinder.

Keywords: Wave propagation; 2D functionally graded materials; Meshless local Petrov-Galerkin method; Thick hollow cylinder.

---

[1] Civil Engineering Department, Faculty of Engineering, Ferdowsi University of Mashhad, Mashhad, Iran

[2] Industrial Engineering Department, Faculty of Engineering, Ferdowsi University of Mashhad, Mashhad, Iran

[3] Corresponding author: Seyed Mahmoud Hosseini, Tel: +98 511 8805064, Fax: +98 511 8763301, E-mails: sm_hoseini@yahoo.com & sm_hosseini@um.ac.ir

1   Introduction

As a new kind of composite materials, functionally graded materials (FGMs) are widely used in some industries with thermal applications. FGMs are made by combination of two different materials such as ceramic and metal, which its microstructure and mechanical properties are vary continuously and smoothly from one material to the other. One of the most important research topics in FGMs is wave propagation and dynamic analysis of structures made of FGMs, which some researches have been carried out in the recent years. The stress wave propagation [Liu, Han, and Lam (1999)], analysis of one dimensional wave propagation [Chiu and Erdogan (1999)], designing of FGMs based on management of stress waves [Bruck (2000)] and dynamic analysis of FG structures under impulsive loading [Li, Ramesh, and Chin (2001)] can be listed as some of previous works. By using laminate plate theory, the behaviors of waves including scattering were studied in a FG elastic plate by Chen et al. [Hosseini, Akhlaghi, and Shakeri (2007)]. Hosseini et al. [Chen, Wang, and Bao (2007)] studied on wave propagation and dynamic analysis of FG thick hollow cylinder under mechanical shock loading using linear FG element for a hybrid numerical method based on Galerkin finite element and Newmark finite difference methods. Also, there are some analytical methods to simulate the elastic wave propagation in FG structures that one of them was presented by Hosseini and Abolbashari [Hosseini and Abolbashari (2010)]. Their presented analytical method was based on the combination of Bessel's functions. From engineering perspective, to have a safe design based on high reliability in structures especially in FG structures, some uncertainties in materials should be considered in engineering analysis. Some researches have focused on stochastic analysis of elastic and thermal wave propagation in structures and also dynamic analysis considering uncertainty in mechanical properties. The thermoelastic wave propagation was stochastically studied using an hybrid numerical method (GFE, NFD and Monte Carlo simulation) for isotropic and functionally graded thick hollow cylinder by Hosseini and Shahabian [Hosseini and Shahabian (2011b), Hosseini and Shahabian (2011a)]. Recently, functionally graded materials with two dimensional grading patterns are employed in some industrial applications. Dynamic analysis of functionally graded thick hollow cylinder with finite length and two-dimensional grading patterns under impact loading was studied by Asgari et al [Asgari, Akhlaghi, and Hosseini (2009)]. In their work, the finite element method with graded material properties within each element is used to model the structure, and the Newmark direct integration method is employed to solve the problem in time domain. The hybrid numerical method based on Galerkin finite element (for spatial variables) and Newmark finite difference (for time domain) was successfully used for heat wave propagation and coupled thermoelasticity without energy

dissipation in functionally graded thick hollow cylinder of infinite and finite lengths based on Green–Naghdi theory by Hosseini et al. [Hosseini, Akhlaghi, and Shakeri (2008), Hosseini (2009)].

Some mesh-free and meshless methods such as meshless local Petrov-Galerkin (MLPG) method have become very useful and effective solving methods in engineering problems because these methods don't require to the mesh generation on the domain. The MLPG concept was presented first by Atluri and Zhu [Atluri and Zhu (1998)]. They are solved elasto-static problems in two dimensional domains. A local boundary integral equation formulation in Laplace-transform domain with a meshless approximation, based on the meshless local Petrov-Galerkin (MLPG) method, was successfully implemented by Sladek et al. [Sladek, Sladek, and Zhang (2003)] to solve transient elastodynamic initial-boundary value problems in continuously non-homogeneous solids. In their work, the moving least squares (MLS) method is used for interpolation and the modified fundamental solution as the test function. The bending, buckling and free vibration of Timoshenko nanobeams were studied using the elasticity theory of Eringen and a meshless method by Roque et al. [Roque, Ferreira, and Reddy (2011)]. Two MLPG formulations based on Heaviside step functions and Gaussian weight functions were presented to analyze the dynamic behaviour of elastic and elastoplastic solids by Soares Jr. et al. [Soares, Sladek, and Sladek (2009)]. For both their formulations, a MLS interpolation scheme was adopted, rendering a matricial time-domain system of second order ordinary differential equations. In another research, they [Soares, Sladek, and Sladek (2010)] used their presented method for analysis of the dynamic behavior of elastic and elastoplastic solids. Also, the propagation of thermoelastic waves in a FG thick hollow cylinder and coupled thermoelasticity analysis considering without and with Gaussian uncertainty in mechanical properties were studied by Hosseini et al. [Hosseini, Sladek, and Sladek (2011), Hosseini, Shahabian, Sladek, and Sladek (2011)] using meshless local Petrov-Galerkin (MLPG) method.

It is very difficult to simulate the breakage of material into a large number of fragments as some mesh based methods such as FEM is essentially based on continuum mechanics, in which the elements formulated cannot be broken. The mesh generation is usually leads to a misrepresentation of the breakage path. Serious error can occur because the nature of mechanical properties in FGMs is nonlinear, and therefore the results are highly path dependent. So, MLPG method can be successfully used for dynamic analysis of FGMs. In other words, MLPG method is a powerful numerical method such as other methods (for example: finite element method, generalized finite difference method,...).

In this paper, two dimensional elastic wave propagation and dynamic analysis are studied in a functionally graded thick hollow cylinder with finite length and two di-

mensional grading patterns using meshless local Petrov-Galerkin (MLPG) method. The mechanical properties of 2D-FG cylinder are simulated by using a nonlinear power function with two dimensional volume fractions. The elastic wave fronts are tracked in two dimensional (r-z) domains for various kinds of grading patterns. Also, the time history of displacement and propagation of elastic waves are discussed in details for various values of exponents in two dimensional volume fractions. The MLPG method shows that it is a very effective method with high accuracy for wave propagation analysis of FGMs with one and two dimensional grading patterns.

2   2D functionally graded materials

In 1D functionally graded cylinder, the mechanical properties are varied through one direction for example in cylinder through radial direction (thickness of cylinder). In new generation of 2D functionally graded materials, the mechanical properties vary through two directions. In this study, the mechanical properties are assumed to vary through radial and axial direction of FG cylinder. Two-dimensional FGMs are usually made by continuous gradation of three or four distinct material phases where one or two of them are ceramics and the others are metal alloy phases, and the volume fractions of the constituents vary as a two dimensional nonlinear functions. The 2D-FG cylinder is considered to be made of a combined metal-ceramic material for which the mixing ratio is varied continuously in the r–z directions from pure ceramic to pure metal.

In the present problem, the inner surface of the 2D-FG cylinder is made of two distinct ceramics and the outer surface of two metals, which the terms "c1", "c2", "m1" and "m2"stand for first ceramic, second ceramic, first metal and second metal, respectively. Also, it is assumed that the terms "r_i", "r_o" and "L" are inner radius, outer radius and length of 2D-FG cylinder, respectively. To show the variation of mechanical properties through two directions ($r-z$), the nonlinear two dimensional volume fractions are employed to simulate the gradation of all mechanical properties. The volume fraction nonlinear functions can be explained as follows

$$V_{c1} = \left[1 - \lambda_r^{n_r}\right]\left[1 - \lambda_z^{n_z}\right] \tag{1}$$

$$V_{c2} = \left[1 - \lambda_r^{n_r}\right]\left[\lambda_z^{n_z}\right] \tag{2}$$

$$V_{m1} = \left[\lambda_r^{n_r}\right]\left[1 - \lambda_z^{n_z}\right] \tag{3}$$

$$V_{m2} = \left[\lambda_r^{n_r}\right]\left[\lambda_z^{n_z}\right] \tag{4}$$

where

$$\lambda_r^{n_r} = \left(\frac{r - r_i}{r_o - r_i} \right)^{n_r} \tag{5}$$

$$\lambda_z^{n_z} = \left(\frac{z}{L} \right)^{n_z} \tag{6}$$

The material properties at an arbitrary point, (r, z) in the 2D-FGM cylinder can be simulated using the rule of mixtures as follows

$$P(r,z) = P_{c1} V_{c1} + P_{c2} V_{c2} + P_{m1} V_{m1} + P_{m2} V_{m2} \tag{7}$$

$$P(r,z) = P_{c1} \left[1 - \lambda_r^{n_r} \right] \left[1 - \lambda_z^{n_z} \right] + P_{c2} \left[1 - \lambda_r^{n_r} \right] \left[\lambda_z^{n_z} \right] \\ + P_{m1} \left[\lambda_r^{n_r} \right] \left[1 - \lambda_z^{n_z} \right] + P_{m2} \left[\lambda_r^{n_r} \right] \left[\lambda_z^{n_z} \right] \tag{8}$$

The term "$P(r,z)$" can be considered as modules of elasticity "E" and density "ρ".

$$E(r,z) = E_{c1} \left[1 - \lambda_r^{n_r} \right] \left[1 - \lambda_z^{n_z} \right] + E_{c2} \left[1 - \lambda_r^{n_r} \right] \left[\lambda_z^{n_z} \right] \\ + E_{m1} \left[\lambda_r^{n_r} \right] \left[1 - \lambda_z^{n_z} \right] + E_{m2} \left[\lambda_r^{n_r} \right] \left[\lambda_z^{n_z} \right] \tag{9}$$

$$\rho(r,z) = \rho_{c1} \left[1 - \lambda_r^{n_r} \right] \left[1 - \lambda_z^{n_z} \right] + \rho_{c2} \left[1 - \lambda_r^{n_r} \right] \left[\lambda_z^{n_z} \right] \\ + \rho_{m1} \left[\lambda_r^{n_r} \right] \left[1 - \lambda_z^{n_z} \right] + \rho_{m2} \left[\lambda_r^{n_r} \right] \left[\lambda_z^{n_z} \right] \tag{10}$$

The presented volume fractions can be calculated at bounding surfaces and corners of cylinder as Table 1 for the presented problem in this paper. The basic constituents of the 2D-FGM cylinder are presented in Table 2.

Table 1: The values of volume fractions at bounding surfaces and corners of cylinder

	$z = 0$				$z = L$			
	V_{c1}	V_{c2}	V_{m1}	V_{m2}	V_{c1}	V_{c2}	V_{m1}	V_{m2}
$r = r_i$	1	0	0	0	0	1	0	0
$r = r_o$	0	0	1	0	0	0	0	1

Table 2: Basic constituents of the 2D-FGM cylinder [Asgari, Akhlaghi, and Hosseini (2009)]

Constituents	Material	$E(GPa)$	ρ (kg/m3)
$m1$	Ti6Al4V	$E_{m1} = 115$	$\rho_{m1} = 4515$
$m2$	Al 1,100	$E_{m2} = 69$	$\rho_{m2} = 2715$
$c1$	SiC	$E_{c1} = 440$	$\rho_{c1} = 3210$
$c2$	Al $_2$O$_3$	$E_{c2} = 300$	$\rho_{c2} = 3470$

3   Mathematical formulations

To show the capability of MLPG method for two dimensional wave propagation analysis in FGMs with two directional grading patterns, the following formulations and modeling are used in this article. Although, the variable kinematics models based on some unified formulation such as very well-known Carrera Unified Formulation (CUF) could be used to assess numerically the proposed technique [Carrera and Ciuffreda (2005), Carrera (2003), Rodrigues, Roque, Ferreira, Cinefra, and Carrera (2012)]. This work furnishes a ground to develop the application of MLPG for dynamic analysis of FGMs using unified formulations (such as CUF).

The axisymmetric geometry and loading conditions are assumed for the problem. Consequently, the equations of motion in a 2D-FG cylinder are given by the following equations to obtain the displacements and stresses.

$$\frac{\partial \sigma_{rr}}{\partial r} + \frac{\sigma_{rr} - \sigma_{\theta\theta}}{r} + \frac{\partial \tau_{rz}}{\partial z} = \rho(r,z)\frac{\partial^2 u_r}{\partial t^2} \tag{11}$$

$$\frac{\partial \tau_{rz}}{\partial r} + \frac{\partial \sigma_{zz}}{\partial z} + \frac{\tau_{rz}}{r} = \rho(r,z)\frac{\partial^2 u_z}{\partial t^2} \tag{12}$$

where "σ_{rr}", "$\sigma_{\theta\theta}$", "σ_{zz}" and "τ_{rz}" are radial, hoop, axial and shear stresses, respectively. The terms "u_r" and "u_θ" stand for radial and axial displacements. The stress-strain relations are given as

$$\sigma = [D]\,\varepsilon \tag{13}$$

where

$$\sigma^T = \left\{ \begin{array}{cccc} \sigma_{rr} & \sigma_{\theta\theta} & \sigma_{zz} & \tau_{rz} \end{array} \right\} \tag{14}$$

and

$$\varepsilon^T = \left\{ \begin{array}{cccc} \varepsilon_{rr} & \varepsilon_{\theta\theta} & \varepsilon_{zz} & \varepsilon_{rz} \end{array} \right\} \tag{15}$$

The matrix "*D*" is given for 2D-FGM as follows

$$[D] = \frac{E\,(r,z)}{(1+v)\,(1-2v)} \begin{bmatrix} 1-v & v & v & 0 \\ v & 1-v & v & 0 \\ v & v & 1-v & 0 \\ 0 & 0 & 0 & \frac{1-2v}{2} \end{bmatrix} \tag{16}$$

and also we have

$$\varepsilon_{rr} = \frac{\partial u_r}{\partial r}, \quad \varepsilon_{\theta\theta} = \frac{u_r}{r}, \quad \varepsilon_{zz} = \frac{\partial u_z}{\partial z}, \quad \varepsilon_{rz} = \frac{\partial u_z}{\partial r} + \frac{\partial u_r}{\partial z} \tag{17}$$
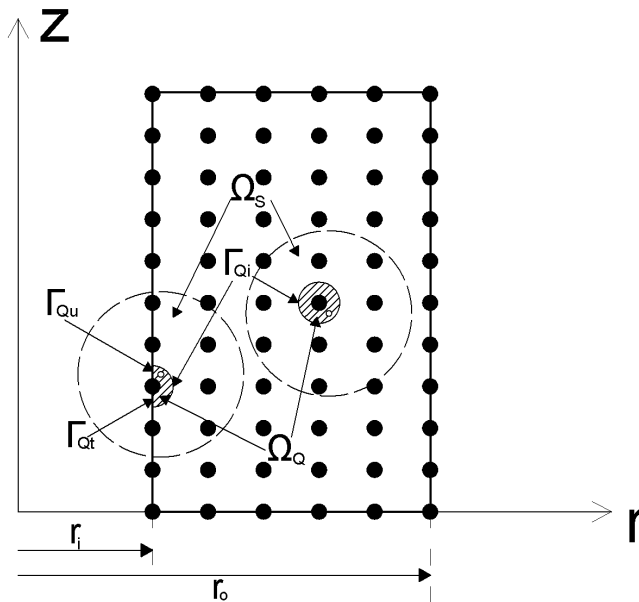
Figure 1: A sketch of quadrature domain

In the MLPG method, the global domain of the problem is divided to many sub-domains, which a weak-form over the local sub-domains such as "Ω_Q" is constructed [Atluri (2004)]. These sub-domains can be overlapping each other, and cover the whole global domain (see Figure 1). The local sub-domains could be of any geometric shape such as circle and rectangular and various size. In the present paper, the local sub-domains are taken to be of a circular shape for simplicity. In such a case the calculation of domain-integrals is quite easy. The local weak-form of the governing equations (3) and (4) for $(r,z) \in \Omega$ can be written as

$$\int_\Omega \left\{ \frac{\partial \sigma_{rr}}{\partial r} + \frac{\sigma_{rr} - \sigma_{\theta\theta}}{r} + \frac{\partial \tau_{rz}}{\partial z} - \rho(r,z)\frac{\partial^2 u_r}{\partial t^2} \right\} \psi_r(r,z,t)\,d\Omega = 0 \tag{18}$$

$$\int_\Omega \left\{ \frac{\partial \tau_{rz}}{\partial r} + \frac{\partial \sigma_{zz}}{\partial z} + \frac{\tau_{rz}}{r} - \rho(r,z)\frac{\partial^2 u_z}{\partial t^2} \right\} \psi_z(r,z,t)\,d\Omega = 0 \tag{19}$$

where "$\psi_r(r,z,t)$" and "$\psi_z(r,z,t)$" are weight or test functions. The sub-domains in axisymmetric cases can be considered as

$$d\Omega = 2\pi r\,d\Omega_Q \tag{20}$$

Therefore the governing equations in weak forms can be rewritten as follows

$$\int_{\Omega_Q} \left\{ \frac{\partial \sigma_{rr}}{\partial r} + \frac{\sigma_{rr} - \sigma_{\theta\theta}}{r} + \frac{\partial \tau_{rz}}{\partial z} - \rho(r,z)\frac{\partial^2 u_r}{\partial t^2} \right\} \psi_r(r,z,t)\,r\,d\Omega_Q = 0 \tag{21}$$

$$\int_{\Omega_Q} \left\{ \frac{\partial \tau_{rz}}{\partial r} + \frac{\partial \sigma_{zz}}{\partial z} + \frac{\tau_{rz}}{r} - \rho(r,z)\frac{\partial^2 u_z}{\partial t^2} \right\} \psi_z(r,z,t)\,r\,d\Omega_Q = 0 \tag{22}$$

Applying the Gauss divergence theorem to equations (21) and (22) one can write

$$\begin{aligned} &\int_{\Gamma_Q} r\Psi_r n_r \sigma_{rr}\,d\Gamma_Q - \int_{\Omega_Q} (\Psi_r + r\Psi_{r,r})\sigma_{rr}\,d\Omega_Q + \int_{\Omega_s} \Psi_r(\sigma_{rr} - \sigma_{\theta\theta})\,d\Omega_Q \\ &+ \int_{\Gamma_Q} r\Psi_r n_z \tau_{rz}\,d\Gamma_Q - \int_{\Omega_Q} \Psi_{r,z}\tau_{rz}\,r\,d\Omega_Q - \int_{\Omega_Q} \Psi_r \rho(r,z)\,r\ddot{u}_r\,d\Omega_Q = 0 \end{aligned} \tag{23}$$

$$\begin{aligned} &\int_{\Omega_Q} (r\Psi_{r,r}\sigma_{rr} + \Psi_r\sigma_{\theta\theta} + r\Psi_{r,z}\tau_{rz})\,d\Omega_Q - \int_{\Gamma_Q} r\Psi_r(n_r\sigma_{rr} + n_z\tau_{rz})\,d\Gamma_Q \\ &+ \int_{\Omega_Q} \Psi_r \rho(r,z)\,r\ddot{u}_r\,d\Omega_Q = 0 \end{aligned} \tag{24}$$

and

$$\int\limits_{\Gamma_Q} r\Psi_z n_r \tau_{rz} d\Gamma_Q - \int\limits_{\Omega_Q} (\Psi_z + r\Psi_{z,r}) \tau_{rz} d\Omega_Q + \int\limits_{\Omega_Q} \Psi_z \tau_{rz} d\Omega_Q$$
$$+ \int\limits_{\Gamma_Q} r\Psi_z n_z \sigma_{zz} d\Gamma_Q - \int\limits_{\Omega_Q} \Psi_{z,z} \sigma_{zz} r d\Omega_Q - \int\limits_{\Omega_Q} \Psi_z \rho\,(r,z)\, r\ddot{u}_z d\Omega_Q = 0 \tag{25}$$

$$\int\limits_{\Omega_Q} (r\Psi_{z,r}\tau_{rz} + r\Psi_{z,z}\sigma_{zz})\, d\Omega_Q - \int\limits_{\Gamma_Q} r\Psi_z\,(n_r\tau_{rz} + n_z\sigma_{zz})\, d\Gamma_Q$$
$$+ \int\limits_{\Omega_Q} \Psi_z \rho\, r\ddot{u}_z d\Omega_Q = 0 \tag{26}$$

The local weak forms (24) and (26) are the starting point for deriving local boundary integral equations on the basis of appropriate test functions. The boundary of quadrature domain can be explained as $\Gamma_Q = \Gamma_{Qi} \cup \Gamma_{Qu} \cup \Gamma_{Qt}$ where "Γ_{Qi}" is the internal boundary of the domain, "Γ_{Qt}" is the part of the natural boundary that intersects with the quadrature domain, and "Γ_{Qu}" is the part of the essential boundary that intersects with the quadrature domain (see Figure 1). The equations (24) and (26) can be taken into account in new form as follows

$$\int_{\Omega_Q} (r\,\psi_{r,r}\sigma_{rr} + \psi_r\,\sigma_{\theta\theta} + r\,\psi_{r,z}\,\tau_{rz})\,d\Omega - \int_{\Gamma_{Qi}} r\,\psi_r(n_r\sigma_{rr} + n_z\tau_{rz})d\Gamma_{Qi}$$
$$- \int_{\Gamma_{Qu}} r\,\psi_r(n_r\sigma_{rr} + n_z\tau_{rz})d\Gamma_{Qu} + \int_{\Omega_Q} r\,\psi_r\rho\,(r,z)\,\frac{\partial^2 u}{\partial t^2}d\Omega = \int_{\Gamma_{Qt}} r\,\psi_r t_r\,d\Gamma_{Qt} \tag{27}$$

$$\int_{\Omega_Q} (r\,\psi_{z,r}\tau_{rz} + r\,\psi_{z,z}\sigma_{zz})d\Omega - \int_{\Gamma_{Qi}} r\,\psi_z(n_r\tau_{rz} + n_z\sigma_{zz})d\Gamma_{Qi}$$
$$- \int_{\Gamma_{Qu}} r\,\psi_z(n_r\tau_{rz} + n_z\sigma_{zz})d\Gamma_{Qu} + \int_{\Omega_Q} r\,\psi_z\rho\,(r,z)\,\frac{\partial^2 w}{\partial t^2}d\Omega = -\int_{\Gamma_{Qt}} r\,\psi_z t_z\,d\Gamma_{Qt} \tag{28}$$

where "t_r" and "t_z" are traction vectors.

4 Mesh-less technique

In mesh-less local Petrov-Galerkin (MLPG) method, a local interpolation is used to represent the trial function with the values (or the fictitious values) of the unknown variable at some randomly located nodes in analyzed domain. In the MLPG method, the test and the trial functions are not necessarily from the same functional spaces. The trial function is chosen to be the interpolation over a number of nodes randomly distributed within the domain of influence. For the spatial distributions of functions "$u_r(r, z, t)$" and "$u_z(r, z, t)$" we apply the mesh-less approximation over a number of nodes randomly distributed within the domain of influence using

the radial basis functions (RBF). Thus, assuming the separation of the radial and axial displacement variables, the considered approximations take the form

$$u_r(r, z, t) = u_r(\bar{r}, t) = R^T(\bar{r}) A(t) \tag{29}$$

$$u_z(r, z, t) = u_z(\bar{r}, t) = R^T(\bar{r}) A(t) \tag{30}$$

where $R^T(\bar{r}) = [R_1(\bar{r}), R_2(\bar{r}), ..., R_n(\bar{r})]$ is the set of radial basis functions centered around "$\bar{r}_I$", and "A" and "B" are vectors containing the coefficients of "A_I" and "B_I", $I = 1, 2, ..., n$. The term "n" is number of distributed nodes.

$$|\bar{r}|^2 = \left(|r - r_I|^2 + |z - z_I|^2 \right) \tag{31}$$

The radial basis function studied in this article is [Sladek, Sladek, Tanaka, and Zhang (2005)]

$$R_I(\bar{r}) = \left(|\bar{r} - \bar{r}_I|^2 + c^2 \right)^{m/2} \tag{32}$$

Form the interpolation equations (29) and (30) for the radial basis functions, the following systems of linear equations for the coefficients "A" and "B" are obtained

$$R_0 A(t) = \hat{u}_r(t) \tag{33}$$

$$R_0 B(t) = \hat{u}_z(t) \tag{34}$$

where

$$\hat{u}_r^T(t) = \left[u_r^1(t), u_r^2(t), ..., u_r^n(t) \right] \tag{35}$$

$$\hat{u}_z^T(t) = \left[u_z^1(t), u_z^2(t), ..., u_z^n(t) \right] \tag{36}$$

are composed of the time variable nodal values of displacements "$u_r^I(t)$" and temperature "$u_z^I(t)$", while R_0 is the matrix defined by nodal values of the RBFs as

$$R_0 = \begin{bmatrix} R_1(\bar{r}_1) & R_2(\bar{r}_1) & ... & R_n(\bar{r}_1) \\ R_1(\bar{r}_2) & R_2(\bar{r}_2) & ... & R_n(\bar{r}_2) \\ \vdots & \vdots & \vdots & \vdots \\ R_1(\bar{r}_n) & R_2(\bar{r}_n) & ... & R_n(\bar{r}_n) \end{bmatrix}. \tag{37}$$

To calculate the vectors "$A(t)$" and "$B(t)$", we can write from equations (33) and (34)

$$A(t) = R_0^{-1} \hat{u}_r(t) \tag{38}$$

$$B(t) = R_0^{-1} \hat{u}_z(t) \tag{39}$$

The approximated functions can be expressed in terms of the nodal values and the shape functions as

$$u_r(\bar{r},t) = R^T(\bar{r}) R_0^{-1} \hat{u}_r(t) = \Phi^T(\bar{r}) \hat{u}_r(t) = \sum_{a=1}^{n} \varphi^a(\bar{r}) u_r^a(t) \tag{40}$$

$$u_z(\bar{r},t) = R^T(\bar{r}) R_0^{-1} \hat{u}_z(t) = \Phi^T(\bar{r}) \hat{u}_z(t) = \sum_{a=1}^{n} \varphi^a(\bar{r}) u_z^a(t) \tag{41}$$

where $\phi^a(\bar{r})$ is the shape function associated with the node a. The nodal shape functions are given by

$$\Phi^T(\bar{r}) = R^T(\bar{r}) R_0^{-1} \tag{42}$$

The equations (40) and (41) can be rewritten in matrix forms as follows

$$U(\bar{r},t) = \left\{ \begin{array}{c} u_r(\bar{r},t) \\ u_z(\bar{r},t) \end{array} \right\} = \sum_{a=1}^{n} \left[\begin{array}{cc} \varphi^a(\bar{r}) & 0 \\ 0 & \varphi^a(\bar{r}) \end{array} \right] \left\{ \begin{array}{c} u_r^a(t) \\ u_z^a(t) \end{array} \right\} = \sum_{a=1}^{n} \Phi^a(\bar{r}) u^a(t) \tag{43}$$

Also, the matrix forms of governing equations (27) and (28) for I^{th} node are given as

$$\int_{\Omega_Q} [\Psi']_I [\sigma] d\Omega_Q - \int_{\Gamma_{Qi}} r [\Psi]_I [n] [\sigma] d\Gamma_{Qi} - \int_{\Gamma_{Qu}} r [\Psi]_I [n] [\sigma] d\Gamma_{Qu} + \int_{\Omega_Q} r [\Psi]_I \rho(r,z) \frac{\partial^2}{\partial t^2} [U] d\Omega_Q = \int_{\Gamma_{Qt}} r [\Psi]_I [t] d\Gamma_{Qt} \tag{44}$$

where

$$[\Psi'] = \left[\begin{array}{cccc} r\,\psi_{r,r} & \psi_r & 0 & r\,\psi_{r,z} \\ 0 & 0 & r\,\psi_{z,z} & r\,\psi_{z,r} \end{array} \right] \tag{45}$$

and

$$[\sigma] = D \sum_{a=1}^{n} [B]^a u^a (t) \tag{46}$$

$$[D] = \frac{E(r,z)}{(1+v)(1-2v)} \begin{bmatrix} 1-v & v & v & 0 \\ v & 1-v & v & 0 \\ v & v & 1-v & 0 \\ 0 & 0 & 0 & \frac{1-2v}{2} \end{bmatrix} \tag{47}$$

$$[B]^a = \begin{bmatrix} \varphi_{,r}^a (\bar{r}) & 0 \\ \frac{\varphi_r^a(\bar{r})}{r} & 0 \\ 0 & \varphi_{,z}^a (\bar{r}) \\ \varphi_{,z}^a (\bar{r}) & \varphi_{,r}^a (\bar{r}) \end{bmatrix} \tag{48}$$

The matrix of weight functions "[Ψ]" is given by

$$[\Psi] = \begin{bmatrix} \psi_r & 0 \\ 0 & \psi_z \end{bmatrix} \tag{49}$$

and the unit outward normal vector on the boundary is

$$[n] = \begin{bmatrix} n_r & 0 & 0 & n_z \\ 0 & 0 & n_z & n_r \end{bmatrix} \tag{50}$$

and also

$$[t] = \begin{bmatrix} t_r \\ t_z \end{bmatrix} \tag{51}$$

Substitution of equation (39) into (37) leads us to the following discrete systems of linear equations for the Ith node.

$$\int_{\Omega_Q} [\Psi']_I \left([D] \sum_{a=1}^{n} [B]^a u^a (t) \right) d\Omega_Q - \int_{\Gamma_{Qi}} r [\Psi]_I [n] \left([D] \sum_{a=1}^{n} [B]^a u^a (t) \right) d\Gamma_{Qi}$$

$$- \int_{\Gamma_{Qu}} r [\Psi]_I [n] \left([D] \sum_{a=1}^{n} [B]^a u^a (t) \right) d\Gamma_{Qu} +$$

$$\int_{\Omega_Q} r [\Psi]_I \rho(r,z) \left(\sum_{a=1}^{n} \Phi^a (\bar{r}) \frac{\partial^2 u^a(t)}{\partial t^2} \right) d\Omega_Q = \int_{\Gamma_{Qt}} r [\Psi]_I [t] d\Gamma_{Qt}$$

$$(52)$$

or

$$
\sum_{a=1}^{n} \left\{ \int_{\Omega_Q} [\Psi']_I [D] [B]^a d\Omega_Q - \int_{\Gamma_{Qi}} r [\Psi]_I [n] [D] [B]^a d\Gamma_{Qi} \right\} u^a(t)
$$
$$
+ \sum_{a=1}^{n} \left\{ - \int_{\Gamma_{Qu}} r [\Psi]_I [n] [D] [B]^a d\Gamma_{Qu} \right\} u^a(t) + \qquad (53)
$$
$$
\sum_{a=1}^{n} \left\{ \int_{\Omega_Q} r [\Psi]_I \Phi^a(\bar{r}) \rho(r,z) d\Omega_Q \right\} \frac{\partial^2 u^a(t)}{\partial t^2} = \int_{\Gamma_{Qt}} r [\Psi]_I [t] d\Gamma_{Qt}
$$

The governing equation in matrix form can be assembled as follows

$$
[M] \{\ddot{u}\} + [K] \{u\} = [F] \qquad (54)
$$

where

$$
[K] = \int_{\Omega_Q} [\Psi']_I [D] [B]^a d\Omega_Q - \int_{\Gamma_{Qi}} r [\Psi]_I [n] [D] [B]^a d\Gamma_{Qi}
$$
$$
- \int_{\Gamma_{Qu}} r [\Psi]_I [n] [D] [B]^a d\Gamma_{Qu} \qquad (55)
$$

$$
[M] = \int_{\Omega_Q} r [\Psi]_I \Phi^a(\bar{r}) \rho(r,z) d\Omega_Q \qquad (56)
$$

$$
[F] = \int_{\Gamma_{Qt}} r [\Psi]_I [t] d\Gamma_{Qt} \qquad (57)
$$

and

$$
u^T = [u^1(t) \ u^2(t) \ ... \ u^n(t)] \qquad (58)
$$

$$
\ddot{u}^T = [\ddot{u}^1(t) \ \ddot{u}^2(t) \ ... \ \ddot{u}^n(t)] \qquad (59)
$$

5 Time domain analysis

There are a number of numerical methods to solve the system of differential equations (47) resulting from the application of the GFD method. In this article, the Newmark time approximation scheme with suitable time step is used, and the time-dependent displacement fields are obtained for the cylinder. Consider the system

to be expressed in terms of non-dimensional time $\bar{t} = t_p$ in which the governing equation of system takes the form

$$[M]\left\{\ddot{u}^{t_p}\right\} + [K]\left\{u^{t_p}\right\} = \left[F^{t_p}\right] \tag{60}$$

Using the initial conditions $\left\{F^0\right\}$ and $\left\{u^0\right\}$, the following equation can be obtained

$$[M]\left\{\ddot{u}^0\right\} = \left\{F^0\right\} - [K]\left\{u^0\right\} \tag{61}$$

The matrices $[K_m]$ and $\left\{F_m^{t_p}\right\}$ are defined as follows:

$$[K_m] = [K] + \frac{1}{\lambda_1 \Delta t^2}[M] \tag{62}$$

$$\left\{F_m^{t_p}\right\} = \left\{F^{t_p}\right\} + \frac{1}{\lambda_1 \Delta t^2}[M]\left(\left\{u^{t_{p-1}}\right\} + \Delta t\left\{\dot{u}^{t_{p-1}}\right\} + (0.5 - \lambda_1)\Delta t^2\left\{\ddot{u}^{t_{p-1}}\right\}\right) \tag{63}$$

The matrices of $[u^{t_p}]$, $[\dot{u}^{t_p}]$, and $[\ddot{u}^{t_p}]$ can be computed using following equations:

$$\left\{u^{t_p}\right\} = [K_m]^{-1}\left\{f_m^{t_p}\right\} \tag{64}$$

$$\left\{\ddot{u}^{t_p}\right\} = \frac{1}{\lambda_1 \Delta t^2}\left(\left\{u^{t_p}\right\} - \left\{u^{t_{p-1}}\right\} - \Delta t\left\{\dot{u}^{t_{p-1}}\right\} - \Delta t^2(0.5 - \lambda_1)\left\{\ddot{u}^{t_{p-1}}\right\}\right) \tag{65}$$

$$\left\{\dot{u}^{t_p}\right\} = \left\{\dot{u}^{t_{p-1}}\right\} + \Delta t\left[(1 - \lambda_2)\left\{\ddot{u}^{t_{p-1}}\right\} + \lambda_2\left\{\ddot{u}^{t_p}\right\}\right] \tag{66}$$

Using aforementioned equations, the matrices of $[u^{t_p}]$, $[\dot{u}^{t_p}]$, and $[\ddot{u}^{t_p}]$ can be obtained for an arbitrary time. The best convergence rate can be achieved in this method by choosing $\lambda_1 = \frac{1}{4}$ and $\lambda_2 = \frac{1}{2}$.

6   Numerical examples and discussions

To show the capability of presented MLPG method in engineering cases, a 2D-FG thick hollow cylinder with finite length is assumed that "$r_i = 0.25\,m$", "$r_o = 0.5\,m$" and "$L = 1\,m$" are considered as inner radius, outer radius and length, respectively. The mechanical properties of 2D-FG cylinder can be found in Table 2. In MLPG

method, unit step functions are chosen for the test functions "Ψ_r" and "Ψ_z" in each sub-domain.

$$\Psi_z(r,z,t) = \Psi_r(r,z,t) = \begin{cases} 1 & at \quad (r,z) \in (\Omega_s \cup \Gamma_s) \\ 0 & at \quad (r,z) \notin \Omega_s \end{cases} \tag{67}$$

If the same boundary conditions with ref. [Hosseini, Akhlaghi, and Shakeri (2007)] are assumed for the problem and also the volume fraction exponents are selected as "$n_r = 0.01$" and "$n_z = 0$", it is possible to compare the obtained results with those reported in ref. [Hosseini, Akhlaghi, and Shakeri (2007)]. Figure 2 shows a good agreement in comparison of results. The following boundary conditions are assumed for the problem to continue the study.
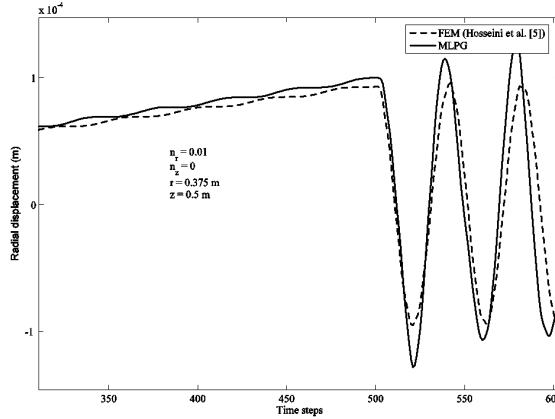
Figure 2: The comparison of obtained results from MLPG with those using FEM for radial displacement

$$\begin{array}{ll} \sigma_r(r_i,z,t) = P(t), & \tau_{rz}(r_i,z,t) = 0 \\ \sigma_r(r_o,z,t) = 0 \quad, & \tau_{rz}(r_o,z,t) = 0 \\ \sigma_z(r,z_0,t) = 0 \quad, & \tau_{rz}(r,z_0,t) = 0 \\ \sigma_z(r,z_L,t) = 0 \quad, & \tau_{rz}(r,z_L,t) = 0 \end{array} \tag{68}$$

where

$$P(t) = \begin{cases} P_0 t & at \quad 0 \leq z \leq \frac{L}{3} \ and \ t \leq 0.005 \ \text{sec} \\ 0 & at \quad \frac{L}{3} \langle z \leq L \ or \ t \rangle \ 0.005 \ \text{sec} \end{cases} \tag{69}$$

It is assumed that "$P_0 = 4\ GPa$". Figure 3 depicts the 2D radial displacement propagation in 2D domain for "$n_r = 0.5$" and "$n_z = 0$" at various times. It is possible to track the contour of wave propagation at various time interval in displacement field of 2D domain (r − z) for one dimensional grading pattern through radial direction. Figure 4 shows us the 2D axial displacement wave propagation in both radial and axial displacement fields for a FG cylinder with one dimensional grading patterns through axial direction for "$n_r = 0$" and "$n_z = 0.5$" at various times. The elastic wave fronts can be tracked as 2D contours in various time intervals in Figure 5 for radial displacement in which the values of volume fraction exponents for FGM with 2D grading patterns are assumed as "$n_r = 0.5$" and "$n_z = 0.5$". It is concluded from Figures 3 to 5 that by increasing the value of volume fraction exponent for a certain direction (axial or radial), the wave propagation speed is decreased. In Figure 6, it is assumed that the grading patterns through both radial and axial directions are similar such as "$n_r = n_z = 0.5$", "$n_r = n_z = 1$" and "$n_r = n_z = 5$". The time histories of radial displacement of middle point on thickness and length are illustrated in Figure 6. It can be seen that by increasing the values of volume fraction exponent, the values of peak points are decreased and the frequency of fluctuations are increased. The time histories of radial displacement are drawn for middle point and various volume fraction exponents in Figure 7.

By considering a fixed value for "n_r" as "$n_r = 0.5$", the time histories of radial displacement of middle point are shown for various values of "n_z" in Figure 8. There is no any significant effect on time histories by increasing the value of "n_z". However, the variation in value of "n_r" create a significant effect on time history of radial displacement, which can be seen in Figure 9. When the value of "n_r" is increased the values of peak points are decreased but the frequency of fluctuation is increased. The similar behaviors with radial displacement can be seen for axial displacement. It means that the variation in value of radial volume fraction exponent "n_r" has a significant effect on dynamic behaviors of displacement comparing to the variation in value of "n_z".

Two sample of 2D distribution of radial displacement through both radial and axial directions are presented in Figures 10 and 11 for "$n_r = n_z = 0.5$" and "$t = 0.065$ sec" and "$t = 0.085$ sec", respectively. Also, the axial displacement distributions in 2D domain (r − z) for "$n_r = n_z = 0.5$" and "$t = 0.065$ sec" are illustrated in Figures 12.

The parameter c is considered to be equal to mean value of minimum distances between nodes along radial and axial directions. The influence of values of this parameter on numerical results is shown in Fig. 13. It is evidence from Fig. 13 that by choosing bigger values for parameter c, the obtained results don't have high accuracy and stability. It is concluded that the selected value for c is the optimum
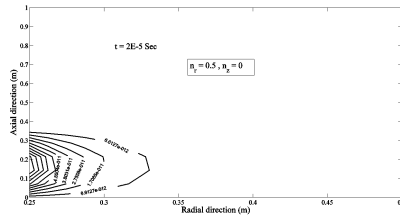
(a)
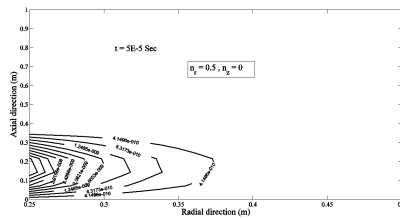
(b)
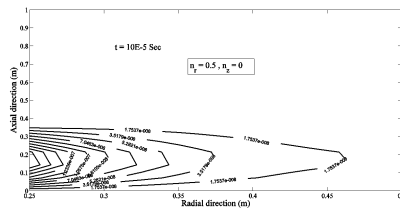
(c)

Figure 3: Two dimensional radial displacement wave propagation for $n_r = 0.5$ and $n_z = 0$ at various times (a) at $t = 2 * 10^{-5}$ sec. (b) at $t = 5 * 10^{-5}$ sec. (c) at $t = 10^{-4}$ sec.

value. Also, a sensitivity analysis are presented for parameter m in Fig .14. It is clear in this figure that the value of m should be less than 2. The shape of soppurt domain is circular. The radius of support domain R_s is assumed to be $R_s = 2.5 \Delta$, which the term Δ is the mean value of minimum distances between nodes along radial and axial directions. It is concluded from Fig. 14 that the selected value for R_s is optimum value. The Fig. 15 shows the influence of R_s on numerical results.

As regards the choice of the size of the time step, it is clear that smaller time steps enable us to get information at shorter time instants with respect to the initial time $t = 0$. For numerical tests, we have chosen two time steps $\Delta t = 10^{-4}$ s and $\Delta t =$
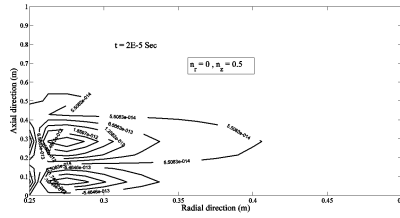
(a)
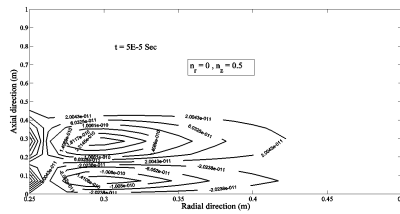
(b)
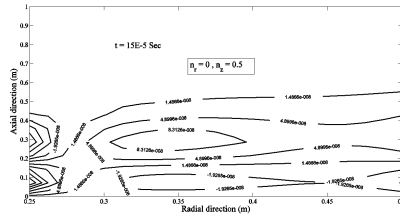
(c)

Figure 4: Two dimensional axial displacement wave propagation for $n_r = 0$ and $n_z = 0.5$ at various times (a) at $t = 2 * 10^{-5}$ sec. (b) at $t = 10^{-4}$ sec. (c) at $t = 1.5 * 10^{-4}$ sec.

10^{-5} s in calculation of two dimensional elastic wave propagation. The distribution of wave fronts at several time instants is plotted in Fig. 16. For time instants to $t < 10^{-4}$ s only the results corresponding to numerical computations with $\Delta t = 10^{-5}$ s are available, but for $t = 10^{-4}$ s and $t = 2 \times 10^{-4}$ s a perfect agreement is achieved for numerical results with using the time steps $\Delta t = 10^{-4}$ s and $\Delta t = 10^{-5}$ s. Therefore, to track the wave fronts in molar concentration and displacement fields at every position, the time step is assumed to be $\Delta t = 10^{-5}$ s. The number of nodes along axial direction N_z^* and along radial direction N_r^* are selected as $N_z^* = 21$ and $N_r^* = 15$. The Figs. 17 and 18 show the influence of various values of N_z^* and
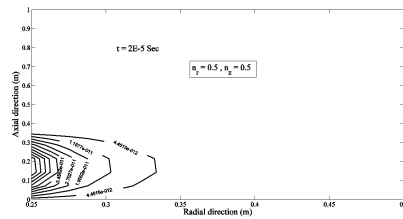
(a)
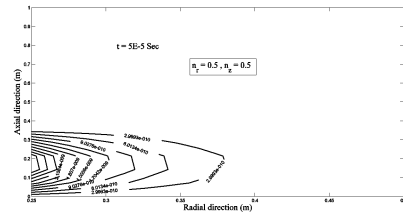
(b)
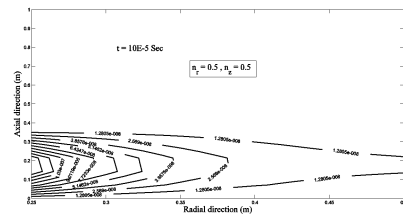
(c)

Figure 5: Two dimensional radial displacement wave propagation for $n_r = 0.5$ and $n_z = 0.5$ at various times (a) at $t = 2 * 10^{-5}$ sec. (b) at $t = 5 * 10^{-5}$ sec. (c) at $t = 10^{-4}$ sec.
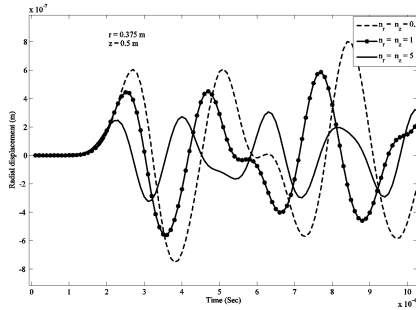
Figure 6: Time history of radial displacement for middle point on thickness and length for $n_r = n_z = 0.5$, $n_r = n_z = 1$ and $n_r = n_z = 5$.
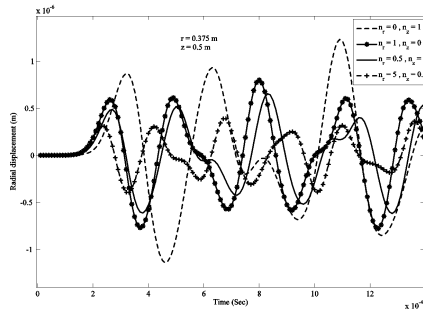
Figure 7: Time history of radial displacement for middle point on thickness and length for various values of n_r and n_z.
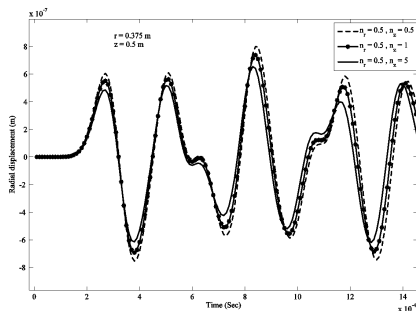
Figure 8: Time history of radial displacement for middle point on thickness and length for certain value of n_r and various values of n_z.
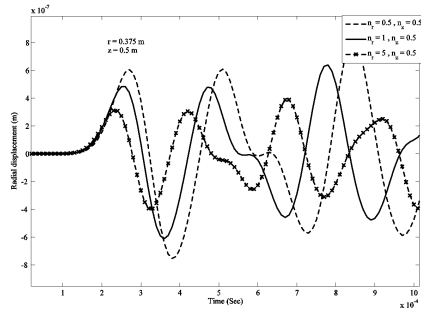
Figure 9: Time history of radial displacement for middle point on thickness and length for certain value of n_z and various values of n_r.
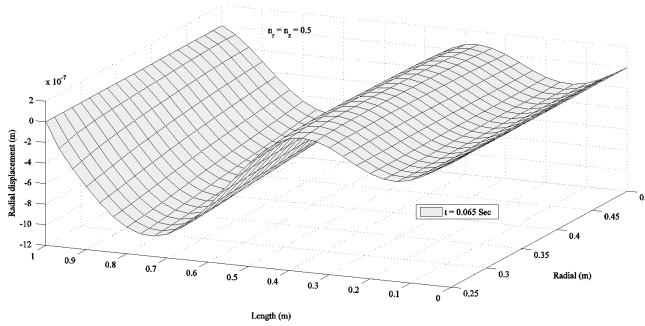
Figure 10: Two dimensional distribution of radial displacement for $n_r = n_z = 0.5$ and $t = 0.065$ sec.
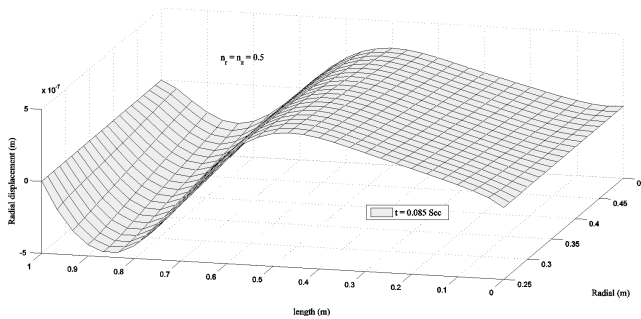
Figure 11: Two dimensional distribution of radial displacement for $n_r = n_z = 0.5$ and $t = 0.085$ sec.
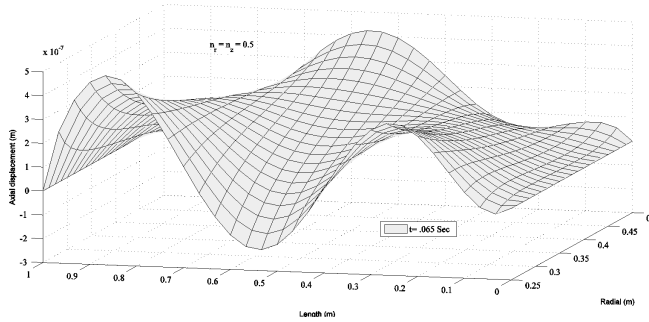
Figure 12: Two dimensional distribution of axial displacement for $n_r = n_z = 0.5$ and $t = 0.065$ sec.
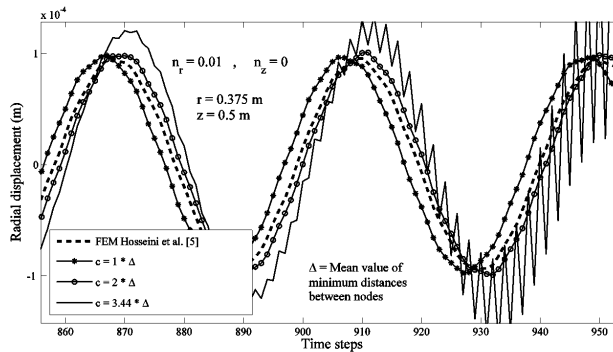
Figure 13: The influence of parameter c on numerical results.

N_r^* on numerical results. It can be concluded that the selected values for N_z^* and N_r^* are optimum values.

As other verifications for presented results and method, the radial and axial stresses are compared with those obtained from finite element method (FEM) [Hosseini, Akhlaghi, and Shakeri (2007)]. A good agreement can be observed from Figs. 19 and 20 between results.

Conclusions:

In this paper, the application of meshless local Petrov-Galerkin (MLPG) method is exploited for dynamic and elastic wave propagation of 2D-FG thick hollow cylinder with 2D nonlinear grading patterns. To simulate the variation of mechanical properties, two dimensional nonlinear volume fractions are presented. The inner surface of 2D-FG thick hollow cylinder is excited by suddenly unloading as mechanical
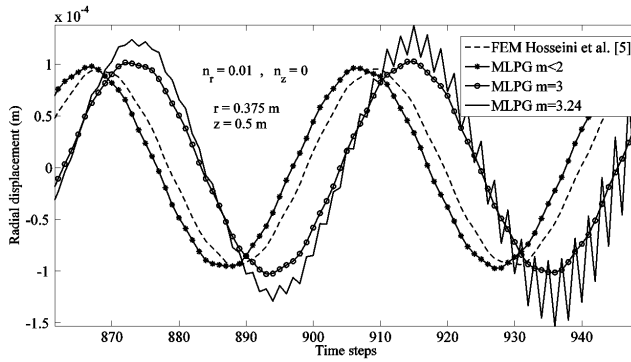
Figure 14: The influence of parameter *c* on numerical results.
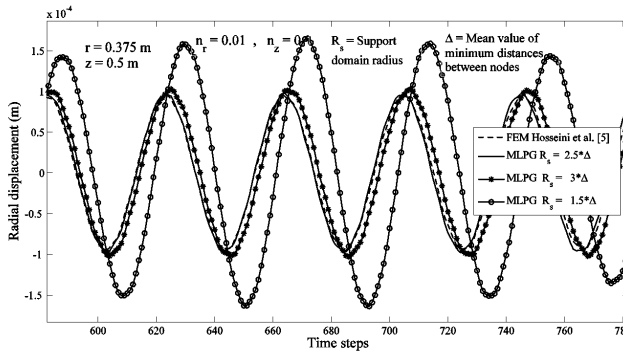
Figure 15: The influence of radius of support domain on numerical results.
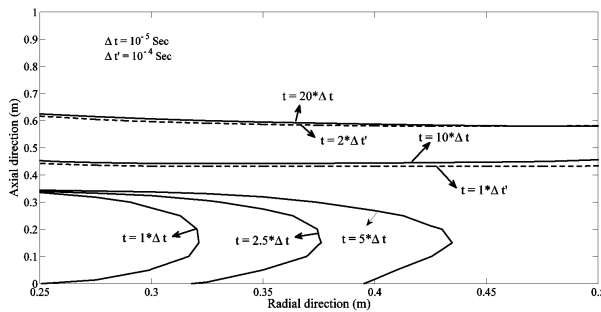
Figure 16: The influence of size of time steps on numerical results.
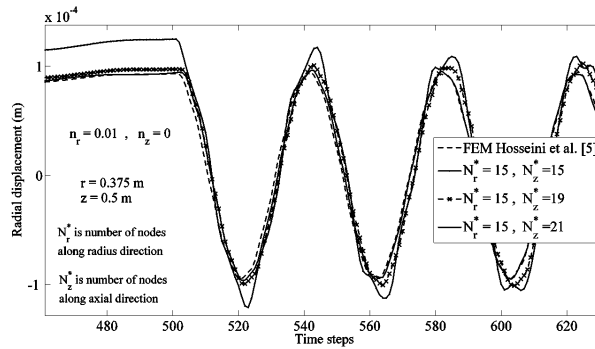
Figure 17: The influence of number of nodes along axial direction on numerical results.
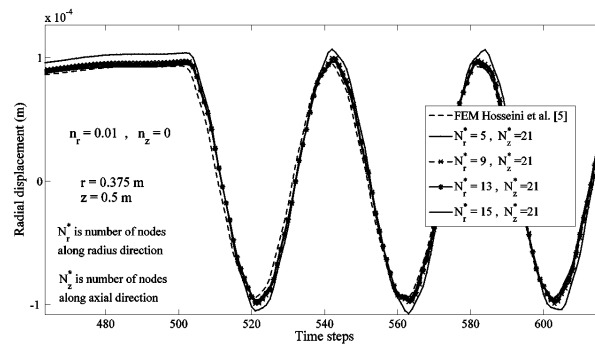
Figure 18: The influence of number of nodes along radial direction on numerical results.

shock loading. To obtain the dynamic behaviors of displacement in time domain, the meshless local Petrov-Galerkin (MLPG) method is combined with Newmark finite difference (NFD) method. The major conclusions resulting from the above analysis can be summarized as follows:

- The 2D wave motion in 2D-FGM is formulated based on meshless local Petrov-Galerkin (MLPG) method for 2D elastic wave propagation analysis.

- The 2D contours of elastic wave fronts are obtained for various kinds of grading patterns in 2D-FGM at various time intervals. It means that the presented method based on MLPG method has a high capability to study dynamic behaviors of FGMs with 2D grading patterns.
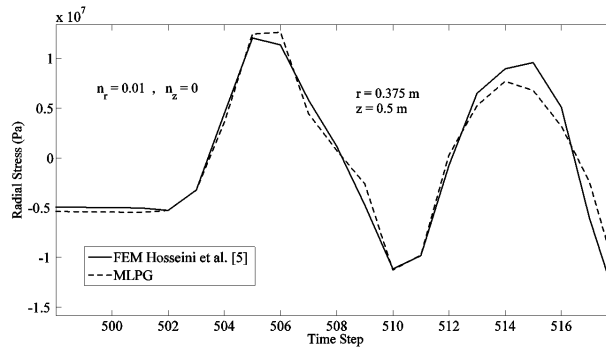
Figure 19: The comparison of obtained radial stresses by MLPG with those obtained by FEM.
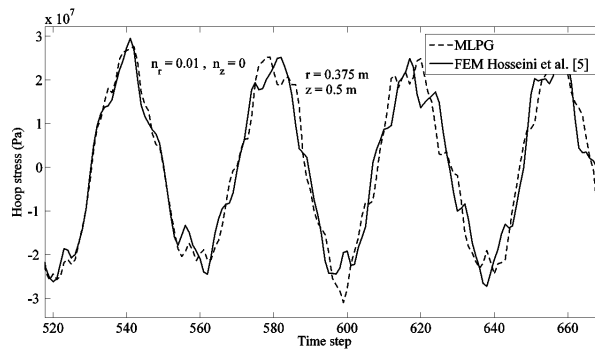
Figure 20: The comparison of obtained axial stresses by MLPG with those obtained by FEM.

- It is possible that the time histories of displacements are assessed for various grading patterns in some points on the body of 2D-FG thick hollow cylinder by using the presented hybrid meshless technique (combined MLPG and NFD method).

- The grading patterns through radial direction have a more effect on time histories of displacements and dynamic behaviors of 2D-FG cylinder comparing to grading patterns through axial direction.

- The presented analysis furnishes a ground for natural frequency analysis of FGMs with two dimensional grading patterns.

References

Asgari, M.; Akhlaghi, M.; Hosseini, S. M. (2009): Dynamic analysis of two-dimensional functionally graded thick hollow cylinder with finite length under impact loading. *Acta Mech*, vol. 208, pp. 163–180.

Atluri, S. N. (2004): *The Meshless Method (MLPG) for Domain and BIE Discretizations.* Tech Science Press: Encino.

Atluri, S. N.; Zhu, T. (1998): A new meshless local petrov–galerkin (mlpg) approach in computational mechanics. *Computation Mechanics*, vol. 24, pp. 348–372.

Bruck, H. A. (2000): A one-dimensional model for designing functionally graded materials to manage stress waves. *Int. J. Solids Struct*, vol. 37, pp. 6383–6395.

Carrera, E. (2003): Theories and finite elements for multilayered plates and shells: A unified compact formulation with numerical assessment and benchmarking. *Archives of Computational Methods in Engineering*, vol. 10, pp. 215–297.

Carrera, E.; Ciuffreda, A. (2005): A unified formulation to assess theories of multilayered plates for various bending problems. *Composite Structures*, vol. 69, no. 3, pp. 271–293.

Chen, W. Q.; Wang, H. M.; Bao, R. H. (2007): On calculating dispersion curves of waves in a functionally graded elastic plate. *Compos Struct*, vol. 81, no. 233–242.

Chiu, T. C.; Erdogan, F. (1999): One-dimensional wave propagation in a functionally graded elastic medium. *J Sound Vib*, vol. 222, pp. 453–487.

Hosseini, S. M. (2009): Coupled thermoelasticity and second sound in finite length functionally graded thick hollow cylinders (without energy dissipation). *Mater Design*, vol. 30, pp. 2011–23.

Hosseini, S. M.; Abolbashari, M. H. (2010): General analytical solution for elastic radial wave propagation and dynamic analysis of functionally graded thick hollow cylinders subjected to impact loading. *Acta Mech*, vol. 212, pp. 1–19.

Hosseini, S. M.; Akhlaghi, M.; Shakeri, M. (2007): Dynamic response and radial wave propagation velocity in thick hollow cylinder made of functionally graded materials. *Engineering Computations*, vol. 24, no. 3, pp. 288–303.

Hosseini, S. M.; Akhlaghi, M.; Shakeri, M. (2008): Heat conduction and heat wave propagation in functionally graded thick hollow cylinder base on coupled thermoelasticity without energy dissipation. *Heat MassTransfer*, vol. 44, pp. 1477–1484.

Hosseini, S. M.; Shahabian, F. (2011):   Stochastic assessment of thermo-elastic wave propagation in functionally graded materials (fgms) with gaussian uncertainty in constitutive mechanical properties. *J Thermal Stresses*, vol. 34, pp. 1071–1099.

Hosseini, S. M.; Shahabian, F. (2011):   Transient analysis of thermo-elastic waves in thick hollow cylinders using a stochastic hybrid numerical method, considering gaussian mechanical properties. *Appl Math Model*, vol. 35, pp. 4697–4714.

Hosseini, S. M.; Shahabian, F.; Sladek, J.; Sladek, V. (2011):   Stochastic meshless local petrov-galerkin (mlpg)method for thermo-elastic wave propagation analysis in functionally graded thick hollow cylinders.   *CMES*, vol. 71, no. 1, pp. 39–66.

Hosseini, S. M.; Sladek, J.; Sladek, V. (2011):   Meshless local petrov-galerkin method for coupled thermoelasticity analysis of a functionally graded thick hollow cylinder.   *Engineering Analysis with Boundary Element*, vol. 35, no. 6, pp. 827–835.

Li, Y.; Ramesh, K. T.; Chin, E. S. C. (2001):   Dynamic characterization of layered and graded structures under impulsive loading.   *Int. J. Solids Struct*, vol. 38, pp. 6045–6061.

Liu, G. R.; Han, X.; Lam, K. Y. (1999):   Stress waves in functionally gradient materials and its use for material characterization.   *Compos Part B Eng*, vol. 30, pp. 383–394.

Rodrigues, J. D.; Roque, C. C.; Ferreira, A. J. M.; Cinefra, M.; Carrera, E. (2012):   Radial basis functions-differential quadrature collocation and a unified formulation for bending, vibration and buckling analysis of laminated plates, according to murakami's zig-zag theory.   *Computers & Structures*, vol. 90-91, pp. 107–115.

Roque, C. M. C.; Ferreira, A. J. M.; Reddy, J. N. (2011):   Analysis of timoshenko nanobeams with a nonlocal formulation and meshless method.   *International Journal of Engineering Science*, vol. 49, pp. 976–984.

Sladek, J.; Sladek, V.; Zhang, C. (2003):   Application of meshless local petrov-galerkin (mlpg) method to elastodynamic problems in continuously nonhomogeneous solids.   *CMES*, vol. 4, no. 6, pp. 637–647.

Sladek, V.; Sladek, J.; Tanaka, M.; Zhang, C. (2005):   Transient heat conduction in anisotropic and functionally graded media by local integral equations. *Eng Anal Bound Elem*, vol. 29, pp. 1047–1065.

Soares, J. D.; Sladek, J.; Sladek, V. (2009):   Dynamic analysis by meshless local petrov-galerkin formulations considering a time-marching scheme based on implicit green's functions. *CMES*, vol. 50, no. 2, pp. 115–140.

Soares, J. D.; Sladek, J.; Sladek, V. (2010):   Non-linear dynamic analyses by meshless local petrov–galerkin formulations. *Int. J. Numer. Meth. Engng*, vol. 81, pp. 1687–1699.